Earth and Planetary Science Letters 450 (2016) 29–39

Contents lists available at ScienceDirect

Earth and Planetary Science Letters

www.elsevier.com/locate/epsl

High-resolution images above the Pampean flat slab of Argentina (31–32°S) from local receiver functions: Implications on regional tectonics

Jean-Baptiste Ammirati [a,*], Sofía Pérez Luján [a,1], Patricia Alvarado [a], Susan Beck [b], Sebastián Rocher [c], George Zandt [b]

[a] Centro de Investigaciones de la Geósfera y Biósfera (CIGEOBIO-CONICET), Universidad Nacional de San Juan, Argentina
[b] Department of Geosciences, University of Arizona, USA
[c] Centro Regional de Investigaciones y Transferencia Tecnológica de La Rioja (CRILAR-CONICET), Argentina

ARTICLE INFO

Article history:
Received 12 January 2016
Received in revised form 9 June 2016
Accepted 10 June 2016
Available online xxxx
Editor: P. Shearer

Keywords:
Andean retroarc
subduction
body waves
surface waves
Eclogite
South America

ABSTRACT

In the flat slab region of the South Central Andes (~31–32°S), geological observations suggest that the regional crustal structure is inherited from the accretion of different terranes during the Ordovician. These structures were later reactivated, first in extension during the Triassic and later in compression during the Andean uplift since the Miocene. Seismological observations confirmed that those fault structures extend to depth with décollement levels that accommodate current crustal shortening in the region. In order to get better insight on the regional tectonics we computed higher frequency receiver functions (RF) from local slab seismicity of intermediate ~100 km depth. Using a common conversion point (CCP) stacking method we obtained cross sections showing high vertical resolution crustal structure at the transition between the Precordillera and the Frontal Cordillera. In addition we performed a joint inversion of our high frequency RFs with surface wave data from ambient noise tomography allowing us to constrain absolute seismic wave velocities. Our higher resolution images reveal more structural details down to a depth of 80 km and laterally over the flat slab in good agreement with previous studies. Our results help to better identify very shallow discontinuities in seismic velocities. Recent petrological analyses combined with our high-resolution RF structure correlates with a crustal mafic composition and partial eclogitization in the lower crust. We observe a shift in the crustal structure between the Precordillera (east) and the Frontal Cordillera (west). Regional seismicity and previously determined focal mechanisms superimposed over our images indicate this shifting is a thrust structure extending down to a depth of 40 km. Our results suggest the presence of a master fault between the Cuyania (Western Precordillera) and Chilenia (Frontal Cordillera) terranes that probably accommodates the crustal deformation in the Pampean flat slab region since the Late Ordovician.

1. Introduction and geological setting

Between 30° and 33°S, the tectonics of the South American western margin is characterized by a series of foreland uplifts related to the flat subduction of the Nazca plate under the South American plate (Ramos, 1988). Well recorded in the South Central Andes segment (30–33°S), the structural, magmatic and sedimentary response to the Cenozoic slab flattening has been intensely studied over the years and, combined with seismological observations, has defined the Pampean (Chilean) flat slab region in time and space (e.g. Stauder, 1973; Allmendinger et al., 1990; Kay and Abbruzzi, 1996; Ramos et al., 2002; Anderson et al., 2007).

The flat slab region is composed of three main morphostructural units (Fig. 1): i) The eastern Sierras Pampeanas (in the Pampia terrane), ii) The Precordillera and the western Sierras Pampeanas (Cuyania terrane) and iii) the Cordillera (Chilenia terrane), which includes the Frontal Cordillera (east) and the Principal Cordillera (west). Regional tectonics involves the Famatinian (Early Ordovician–Early Carboniferous), Gondwanic (Early Carboniferous–Early Cretaceous) and Andean (Early Cretaceous–present) orogenic cycles (Ramos, 1988).

The western Sierras Pampeanas (WSP) are characterized by tilted blocks of Mesoproterozoic ultramafic and mafic rocks, mainly

* Corresponding author.
E-mail address: jb.ammirati@unsj-cuim.edu.ar (J.-B. Ammirati).
[1] Now at Instituto de Estudios Andinos Don Pablo Groeber (IDEAN-CONICET), Universidad de Buenos Aires, Argentina.

http://dx.doi.org/10.1016/j.epsl.2016.06.018
0012-821X/

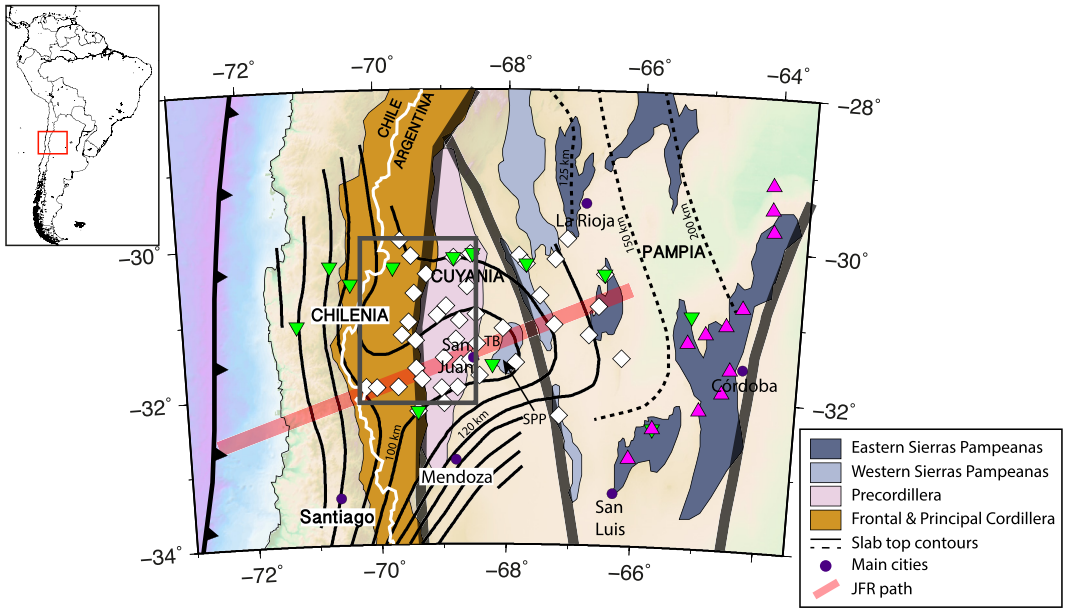

Fig. 1. Location map centered on the Pampean flat slab region of Argentina. The thick black lines mark terrane boundaries (Ramos et al., 2002). Slab top contours are shown by thin black lines (Anderson et al., 2007) and thin black dashed lines (Mulcahy et al., 2014). The white diamonds mark the location of the SIEMBRA seismic stations. The upside-down green triangles mark the location of the CHARGE stations and the magenta triangles mark the location of the ESP stations. The red line shows the path of the JFR under the South American plate (Yáñez et al., 2002). SPP stands for Sierra de Pie de Palo in the western Sierras Pampeanas. The square shows the emplacement of Fig. 2. (For interpretation of the references to color in this figure legend, the reader is referred to the web version of this article.)

metagabbros and garnet-amphibolites well exposed in the Cuyania terrane basement (Kay et al., 1996). The Precordillera is mainly composed of Paleozoic marine carbonate and siliciclastic platform sequences of Cambrian to Devonian ages (Baldis et al., 1982). Western Precordillera rocks consist of slope and deep marine deposits affected by tight folding and low-grade metamorphism (Pérez Luján et al., 2015). The presence of an Ordovician mafic–ultramafic belt that outcrops in the Central and Western Precordillera is generally considered the exposed boundary between the Cuyania and Chilenia terranes (Kay et al., 1984; Davis et al., 1999; Pérez Luján et al., 2015).

The Uspallata–Calingasta valley, a large tectonic depression, separates the Frontal Cordillera from the Precordillera (Fig. 2). Most of the current Frontal Cordillera formed during the Gondwanic orogeny (Neopaleozoic to Triassic times). During this period, the Frontal Cordillera recorded significant extensional tectonics characterized by the Permian–Triassic large plutonic-volcanic Choiyoi Group (Heredia et al., 2002; Rocher et al., 2015). More to the west, the Principal Cordillera is composed of Mesozoic continental and marine deposits exhibiting shallow thin- and thick-skin deformation (La Ramada fold and thrust belt; Cristallini and Ramos, 2000).

Recent focal mechanism solutions (Alvarado et al., 2010; Ammirati et al., 2015) show that the Cuyania–Chilenia boundary is affected by moderate magnitude earthquakes ($4.2 < M_w < 5.4$) with reverse focal mechanisms, down to ∼30 km depth. In this work, we present new higher-resolution crustal velocity structure images for the Pampean flat slab region. We compare our improved crustal velocity structure determined from local slab earthquake receiver functions and ambient noise with petrological analyses. In particular, we investigate the transition zone between the Cuyania and Chilenia terranes in order to propose a seismotectonic model that could explain the current configuration of this boundary in terms of rock composition and tectonic evolution.

2. Previous works

For this study we mainly used IRIS-PASSCAL data from the Sierras Pampeanas Experiment using a Multicomponent Broadband Array (SIEMBRA). This experiment consists in 43 broadband stations deployed in the Pampean flat slab region in December 2007 and operated for two years. The CHile-ARgentina Geophysical Experiment (CHARGE) deployed in the region in 2001 also allowed us to compute some good quality local RFs beneath the Sierra de Pie de Palo (station JUAN: 31.60°S; 68.23°W) in the western Sierras Pampeanas (Fig. 1). Another seismic experiment deployed in 2008–2010 in the eastern Sierras Pampeanas (the ESP experiment) was not directly used for the computation of RFs in this work but contributed to determine phase velocity dispersion from ambient noise tomography (Porter et al., 2012), which we jointly inverted with our local RFs to obtain absolute shear-wave velocities (Fig. 1 & S1).

The aforementioned experiments deployed in the Pampean flat slab region contributed to better understand the flat subduction geometry and the associated tectonic response of the overriding plate. For example, Anderson et al. (2007) analyzed the slab seismicity recorded during the CHARGE experiment to propose new slab top contours refining those determined by Cahill and Isacks (1992) and showing nicely how the flat portion of the subducting slab coincides with the projection of the path of the Juan Fernández Ridge (JFR) under the South American plate (Fig. 1).

Using the same data, Wagner et al. (2005) and Porter et al. (2012) have performed body wave and ambient noise tomography (ANT) respectively, and proposed interpretations about how the flat portion of the subducting slab is probably still hydrated and contrasts with the overlying drier and cooler mantle wedge. Teleseismic RF and converted-wave analysis (Regnier et al., 1994; Gilbert et al., 2006; Perarnau et al., 2010; Gans et al., 2011; Ammirati et al., 2013, 2015) show an abnormally thick crust for the western Cuyania terrane (∼65 km). Some of these studies have observed high shear-wave velocity for depths greater than 40 km likely associated with partial eclogitization in the lower crust. Most of these RF studies also reveal the presence of mid-crustal discontinuities associated with regional seismicity and décollements accommodating global shortening at crustal levels.

Although the crustal structure of the Sierras Pampeanas and the Precordillera has been extensively studied, the western part of the

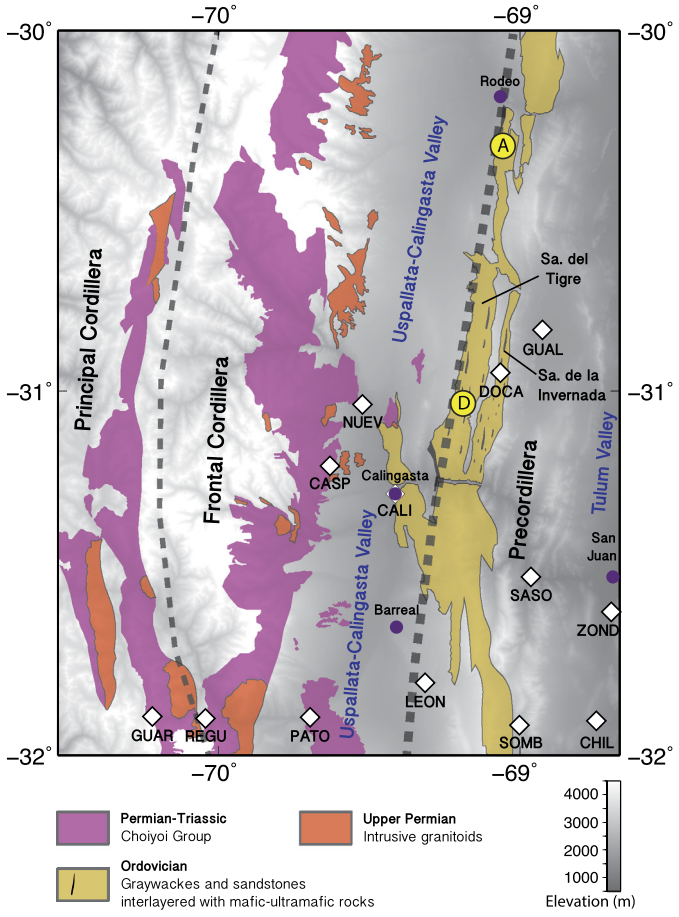

Fig. 2. Main geological formations characterizing the Cuyania–Chilenia boundary simplified from Ragona et al. (1995). The white diamonds mark the location of the SIEMBRA stations used to compute the local RFs presented in this work. The thick grey dashed line marks the approximate boundary between the Cuyania terrane to the east and the Chilenia terrane to the west. This boundary is generally associated with the presence of a belt of mafic–ultramafic rocks that outcrops in the Western and Central Precordillera. The thin grey dashed line delimitates the Frontal Cordillera from the Principal Cordillera. Letters A and D refer to the pictures shown in Fig. 7a & d.

Pampean flat slab region, especially the transition zone between Cuyania and Chilenia and the Frontal Cordillera remain poorly interpreted in terms of seismic velocity structure.

Some studies have focused on regional rock composition and seismic characteristics in terms of wave velocities. For example, Castro de Machuca et al. (2012) have determined the main mineral assemblages for the most representative rocks from the Sierra de Pie de Palo complex (WSP) compared with a database of typical subduction rocks and estimated their physical and seismic properties. Assuming pressure–temperature (P–T) peak metamorphic conditions, the results were then compared with a regional velocity model obtained by Perarnau et al. (2010) to estimate rock facies as a function of depth. They concluded that the lower crust deeper than 28 km depth had high S-wave velocities and low V_p/V_s representative of crustal densification and mafic rocks in the upper amphibolite to granulite/eclogite facies. Exploring P- and S-wave crustal velocities, Venerdini et al. (2016) have confirmed these observations.

Similar studies were performed to the west in the Central and Western Precordillera by Pérez Luján et al. (2015). Shear-wave velocity estimations obtained by them from representative rock samples collected in the Sierra de la Invernada, Sierra del Tigre and Rodeo areas (Fig. 2), can be projected to depths greater than 30 km strengthening the hypothesis of a mafic–ultramafic composition for the middle and lower crust beneath the Central and Western Precordillera. Their results support the idea of a deformed mafic–ultramafic belt at the transition zone between the Precordillera and the Frontal Cordillera extending in depth to levels deeper than 50 km. Boedo et al. (2013) show how the same exposed belt extends in the south to about 33°S where the Precordillera ends.

In this study we combine high-frequency RF, ANT dispersion data and petrological analyses to better constrain the Cuyania–Chilenia terrane boundary.

3. Data and methods

3.1. Local receiver functions

RF analysis uses broadband waveforms recorded by a 3-components seismometer to identify P-to-S conversions from discontinuities beneath the station. The waveforms coming from distant earthquakes will cross discontinuities in seismic velocities at a steep angle and generate P- to S-wave conversions that reverberate beneath the receiver. Hence, a receiver function (RF) is a time series of Gaussian pulses where each spike marks a phase arrival (direct wave and/or associated multiples) directly related to the Earth structure (Langston, 1979).

In this study, we compute RFs from local intermediate-depth seismicity. Local earthquakes are characterized by higher frequency content than that one from teleseismic earthquakes; this allows better vertical resolution since high frequency waveforms are sensitive to smaller velocity variations (Calkins et al., 2006; Perarnau et al., 2012). Local seismograms are also characterized by a higher signal-to-noise ratio allowing us to work with lower magnitude earthquakes.

The dataset used in this work corresponds to the slab seismicity (183 events) recorded by the SIEMBRA array between January 2008 and November 2009 (Fig. 3a). For each station, we select earthquakes with a local magnitude M_L greater than 3.0 and an epicentral distance less than 0.7° (∼78 km) from the receiver. The epicentral distance has been calculated considering an average focal depth of 100 km and a maximum incidence angle of 35° allowing the assumption of plane waves and ensuring traces that exhibit no interferences with the possible generation of surface waves (SW). The average number of events per station is 54 with a maximum of 135 at station Río Saso (SASO) in the Central Precordillera and a minimum of 1 at station Los Colorados (COLO) in the Sierras Pampeanas. In general, we expect stations located above the flat portion of the subducting slab to record a higher number of events since many studies concluded that most of the seismicity occurs in the flat portion of the slab at around 100 km depth (Anderson et al., 2007).

Before computing the local RFs, we removed the mean and rotated the north–south and east–west components into radial and tangential components respectively, along the great circle path. Resulting traces were high-pass filtered (corner frequency of 0.5 Hz) to avoid long-period trends. The difference is small comparing RFs obtained from filtered and unfiltered traces since the local waveforms have a higher frequency content (>1 Hz) while long-period trends are more common in the long-period signals (<0.5 Hz). However, we generally observe better quality RFs for filtered traces. To compute local RFs, we use an iterative pulse stripping deconvolution method (Ligorría and Ammon, 1999) with a maximum of 600 iterations or an improvement of the fit between two iterations lower than 0.01%. We use a Gaussian width of 5 in the deconvolution which corresponds to a low-pass filter of corner frequency 2.4 Hz. A higher Gaussian width, such as 10 (5 Hz) resulted in excessively noisy RFs. The Gaussian filter controls the wavelength size, which is directly related to the maximum vertical resolution recoverable. In this work, the RF vertical resolution is ∼0.5 km.

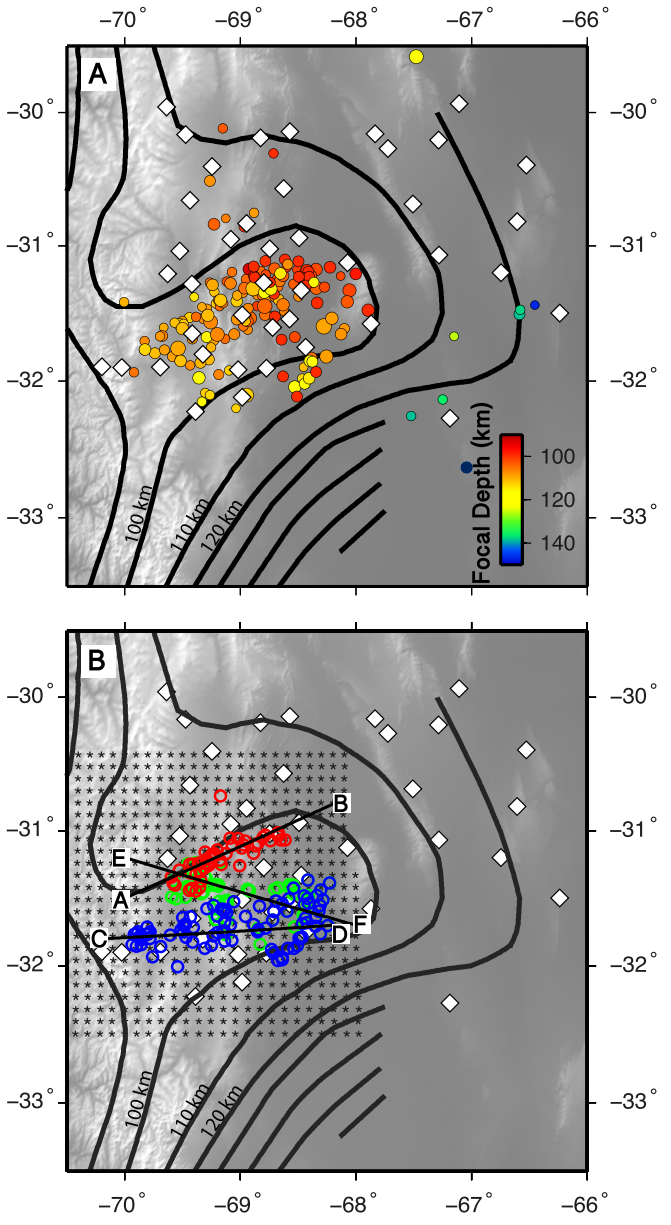

Fig. 3. A) Slab seismicity ($M_L > 3.0$) recorded by the SIEMBRA array (white diamonds). The black lines represent the slab contours (Anderson et al., 2007). Note the regional seismicity is concentrated in the flat portion of the slab. **B)** The colored circles represent the piercing points corresponding to local RFs computed in this work. Red, blue and green correspond to the A–B, C–D and E–F cross sections, respectively. The asterisks mark bin centers for the common conversion point (CCP) stacks. The thick black lines represent the top of the slab contours (Anderson et al., 2007). The black lines indicate the cross sections shown in Fig. 5. (For interpretation of the references to color in this figure legend, the reader is referred to the web version of this article.)

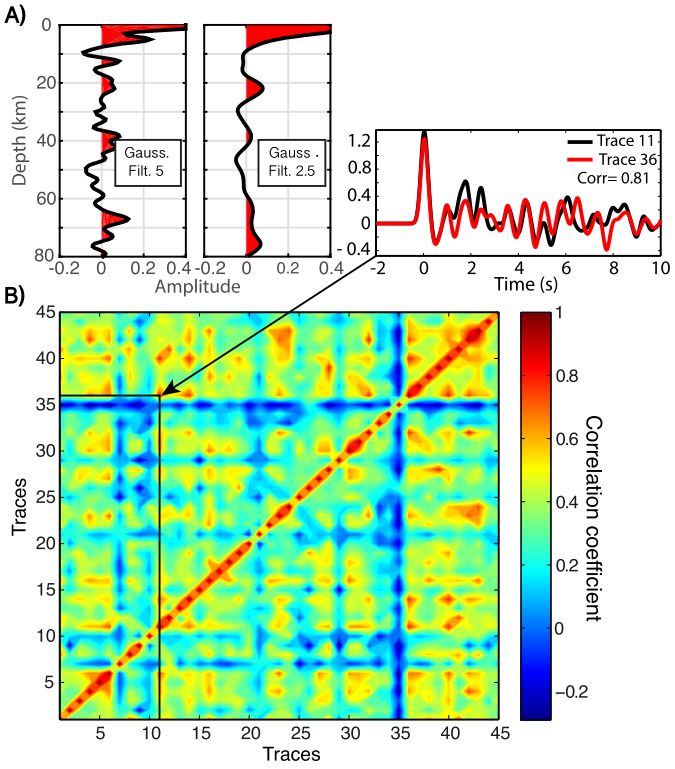

Fig. 4. A) Comparison between local (left, 26 traces) and teleseismic (right, 24 traces) RFs recorded at station DOCA (Central Precordillera). The traces were stacked after moveout correction and time to depth conversion. Local data have been corrected from moveout using the 1D regional velocity model obtained by Ammirati et al. (2015). Teleseismic data are from Ammirati et al. (2013). **B)** Cross correlation matrix. Traces are correlated with one another and return a correlation coefficient value. Pairs of traces with good correlation (correlation coefficient >0.8) are selected. The ensemble of good pairs allows us to identify a waving pattern related to crustal velocity structures and thus differentiate usable traces from noisy and/or poor quality RFs.

The high frequency content of the waveforms combined with a high Gaussian width value used to compute local RFs allows us to image more details at crustal levels in comparison with teleseismic RFs (Fig. 4a). However, this implies more primary conversions and thus, more multiples further back in time, making the RF noisy. Moreover, the deconvolution is much more unstable when using higher frequency waveforms. A challenging aspect consists of differentiating complex traces containing bumps related to the structure from unusable noisy traces. For each station, RFs are thus cross-correlated with each other in order to identify traces exhibiting the same pattern (Fig. 4b). Selected traces were then visually inspected to eventually refine the RF selection. By applying this method, the amount of bad quality RFs is significantly reduced so we are confident that the remaining traces mainly contain information about the structure. Nevertheless, some of the stations lack good quality data. This is the case for stations GUAR and REGU located quite far west and close to our epicentral distance limit criteria. Stations SASO and ZOND also present noisy traces likely due to site effects.

The top of the slab has been imaged in previous studies lying around 95–105 km depth (Gans et al., 2011; Ammirati et al., 2013, 2015). It appears as a strong negative arrival that marks a decrease in seismic velocities due to the presence of likely hydrated oceanic crustal material. Theoretically, high-resolution RFs from the slab would be able to image the top of the slab. However, because the slab top signal is expected 12–13 s after first P-wave arrival, this arrival would be merged with the crustal multiples and thus hard to identify. For this reason we only interpret crustal RF arrivals (between 0 and 80 km depths).

Fig. S2 shows the average radial and tangential RFs obtained after moveout correction for each station used in this work. Theoretically, for wave propagation in a homogenous and isotropic media, we do not expect transverse P-wave signal. The low P-wave amplitudes observed for transverse RFs, in contrast to the corresponding high radial RF amplitudes, support our assumption of homogeneity and isotropy in the sampling region beneath each receiver. Only radial RFs were subsequently stacked.

Once computed and selected, the local RFs are stacked using the Common Conversion Point (CCP) stacking method (details of this methodology can be seen in Dueker and Sheehan, 1997).

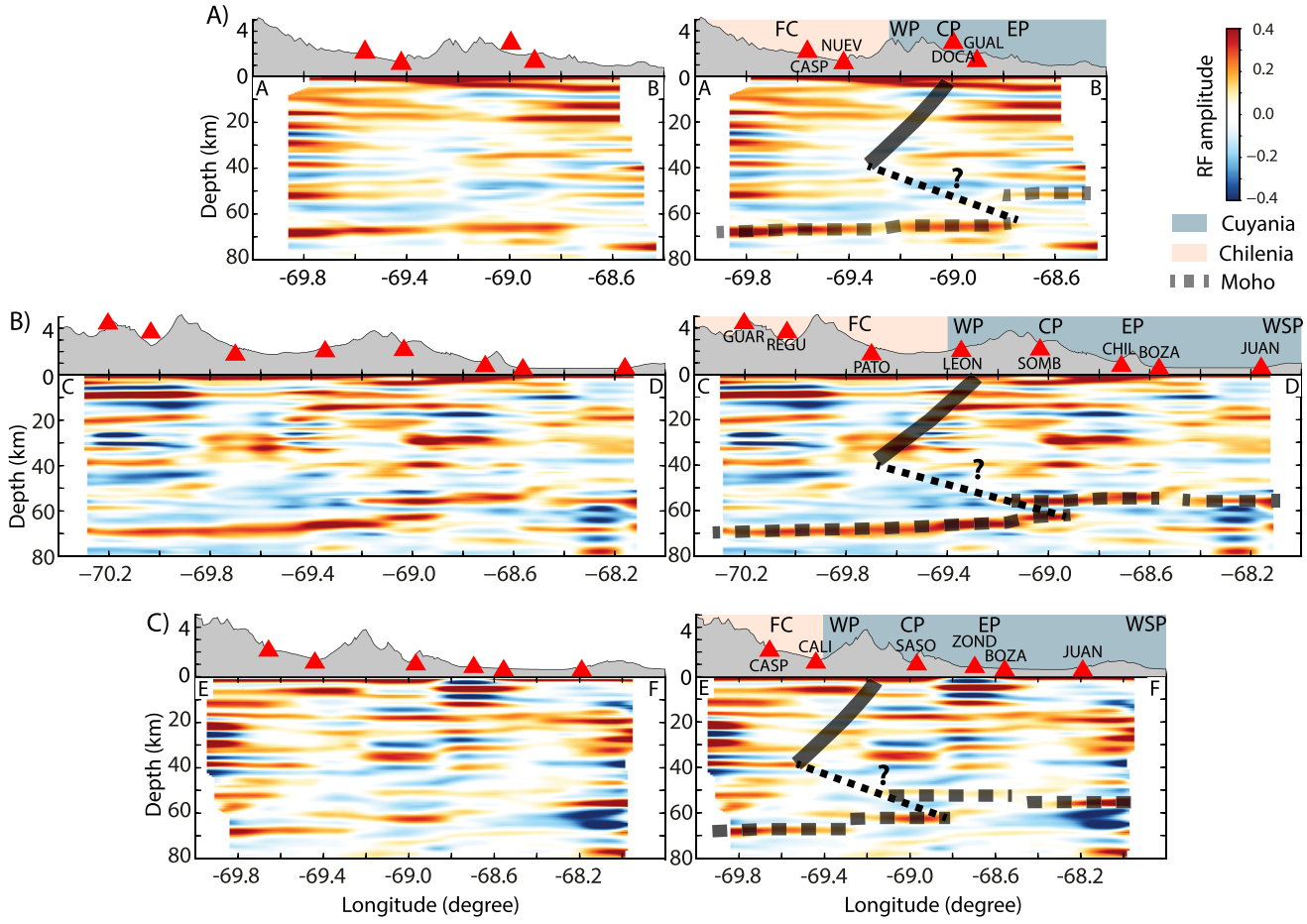

Fig. 5. Cross sections showing our stacked RFs. See Fig. 3 for location of the cross sections. The CCP stacked receiver functions have been projected along the corresponding lines. The time to depth conversion has been performed using the calibrated regional velocity model obtained in Ammirati et al. (2015). Positive amplitudes are in red, negative amplitudes are in blue. Red triangles are the SIEMBRA stations for which we computed the local RFs. FC: Frontal Cordillera; WP: Western Precordillera; CP: Central Precordillera; EP: Eastern Precordillera; WSP: Western Sierras Pampeanas. Note the structure change between the Cuyania and Chilenia terranes indicated by the dark grey line. Our interpretations for the Moho signal correspond to the grey dashed lines. The black dashed line marks a possible shear zone accommodating crustal shortening between the Cuyania and Chilenia terranes in the lower crust. (For interpretation of the references to color in this figure legend, the reader is referred to the web version of this article.)

Briefly, stacking RFs from multiple stations reduces the noise and enhances the conversions and their lateral extent.

Traces are first converted from time to depth using the following travel time equation (Gurrola et al., 1994):

$$\Delta T_{P_s}(z, p, V_s, V_p) = \int_0^z \left(\sqrt{V_s^{-2} - p^2} - \sqrt{V_p^{-2} - p^2}\right) dz \qquad (1)$$

A discretized version of Eq. (1) calculates the travel time delay (ΔT_{P_s}) for each depth increment ($dz_i = 1$ km in our case). Then, RFs are resampled with a point at every time increment to the corresponding depth (z). The process automatically corrects the traces from moveout since the ray parameter (p) of each RF is taken into account. Finally, traces with common conversion points are binned and stacked. In this study, a total of 171 local RFs were stacked. The average number of local RFs is 11 per seismic station and the minimum hit per bin is 5. The common conversion depth has been set to 60 km which corresponds to the average Moho depth in the region of study (Gans et al., 2011; Ammirati et al., 2015). The stacking bins have a radius of 20 km and are spaced by 10 km; hence two bins contain overlapping data, which provide lateral smoothing.

P- and S-wave velocities in Eq. (1) (V_p and V_s, respectively) come from a calibrated velocity model obtained by Ammirati et al. (2015). This model contains crustal details and has been tested for regional seismic source characterization. The uncertainties on the Ammirati et al.'s (2015) crustal seismic velocities (0.3 and 0.2 km/s for P- and S-wave velocities, respectively) cause inaccuracies up to 1.1 s in travel time estimations when applying Eq. (1). Considering an average crustal shear-wave velocity of 3.5 km/s, we estimate the uncertainty on crustal thickness to be ~4 km.

Three CCP cross sections are shown in Figs. 3b and 5. Since wave velocity is expected to increase with increasing depth within the upper plate we chose not to interpret negative arrivals. Those can be either noise-induced or $P_sP_s + P_pS_s$ phases (negative amplitude reverberations).

3.2. Joint inversion

We use the ANT phase velocity dispersion data obtained by Porter et al. (2012) to do a joint inversion with our RF dataset. ANT is more sensitive to crustal shear-wave velocities defining phase velocities for shorter periods (<10 s) and makes it appropriate to combine with high frequency RFs in order to get more detailed absolute velocity structures. Porter et al. (2012) phase velocities are defined for periods ranging from 8 s to 40 s.

For each station, depending on its location, we select the ANT dispersion curve corresponding to the closest grid point on the Porter et al. (2012) model (Fig. S1). Then the RFs are individually inverted with the dispersion data resulting in one velocity model

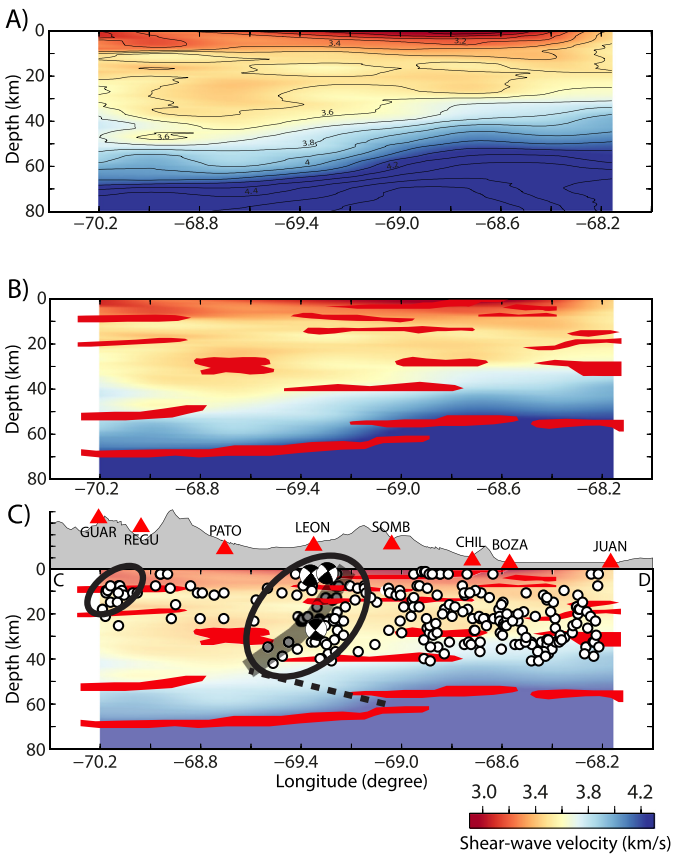

Fig. 6. A) Joint inversion model for the C–D cross section (see Fig. 3b for location). Low velocities appear in red tones, high velocities appear in blue tones. Contour spacing is 0.1 km/s (see main text for details of the joint inversion process). **B)** Same as (A) overlaid with the CCP stack discontinuities shown in Fig. 5b. Note that only positive arrivals interpreted as discontinuities (in the main text) have been reported. **C)** Same as (B) overlaid by regional crustal seismicity (white dots) recorded by the OVA99, CHARSME, CHARGE and SIEMBRA experiments (Linkimer, 2011; Marot et al., 2013). Focal mechanisms are from Ammirati et al. (2015). Clusters of seismic activity related with regional tectonics as discussed in the main text, have been circled. Red triangles represent the seismic stations used for both CCP stacking and joint inversion. (For interpretation of the references to color in this figure legend, the reader is referred to the web version of this article.)

per RF. Those individual velocity models are then averaged to produce the final station S-wave velocity model (Fig. S3). Since all RFs do not fit the data in the same way, the averaged model is weighted with the RF corresponding variance reductions.

We performed the joint inversion using the joint96 code (Julià et al., 2000; Herrmann and Ammon, 2002). The code will iteratively invert the datasets looking for the best velocity model that minimizes both RF and SW residuals. A damping value of 0.5 was chosen as the best compromise between data fit and unrealistic jumps in the resulting model. The p-factor, that controls the influence of each dataset in the joint inversion, has been set to 0.3 which means that the RF dataset accounts for 70% while the ANT dispersion accounts for 30% in the inversion. We observed that keeping the p-factor at low values helps to preserve a good level of details in the resulting model although averaging the models will also have a smoothing effect. Fig. S3 shows the resulting models with 1 standard deviation confidence interval.

The initial velocity model consists of a series of 2-km-thick layers down to 150 km depth characterized by constant seismic wave velocities and density with $V_p = 7$ km/s, $V_p/V_s = 1.75$ and $\rho = 3$ g/cm^3.

Between the stations, the shear-wave velocities have been extrapolated to produce the image shown in Fig. 6a. The RF positive arrivals interpreted as discontinuities in seismic wave velocities (see next section) have been reported in Fig. 6b in order to compare the results from our CCP stacks and from the joint inversion.

4. Results and interpretations

4.1. The Precordillera and western Sierras Pampeanas

In the eastern part of the Pampean flat slab region, beneath the Sierra de Pie de Palo (WSP), we observe a relatively simple shallow structure associated with a relatively high shear-wave velocity (Fig. 5b & 6). This confirms that the structure of the WSP mainly involves cored-based deformation of the Cuyania terrane as illustrated by the rapid uplift of the Sierra Pie de Palo (Fig. 1) with 2 décollement levels around 20 and 30 km depths (Ramos et al., 2002). Those observations are consistent with previous RF results by Calkins et al. (2006) and Perarnau et al. (2010) and P- and S-wave velocity estimations by Venerdini et al. (2016). The S-wave velocity obtained in this sector is consistent with a Cuyania basement mostly characterized by metamorphic rocks in the upper greenschist to amphibolite facies and upper amphibolite to granulite/eclogite facies for rocks located at depths greater than 30 km (Castro de Machuca et al., 2012).

To the west, beneath the Eastern Precordillera several discontinuities are observable at very shallow depths (<10 km) associated with low S-wave velocities ($V_s < 3.2$ km/s) (Fig. 6), generally associated with sedimentary rocks (Brocher, 2005). In our study region, the Eastern Precordillera outcrops are mainly composed of Cambrian limestones (Marquesado Group) compatible with such low S-wave velocities. These limestones mainly expose west-verging faulting extending beneath the Tulum Valley to the east (Fig. 2), which is filled with Tertiary deposits (Baldis et al., 1982). According to our results, we interpret the Tulum basin deposits to be ∼5 km thick (corresponding to the $V_s < 3.0$ km layer) and the base of the Ordovician stratatification at ∼10 km depth, corresponding to a décollement level that separates the sedimentary strata from the Cuyania basement. At deeper levels beneath the Eastern Precordillera we observe the lateral continuation of the 32 km discontinuity that deepens to ∼40 km depth toward the northwest as observable along the cross section E–F (Fig. 5c).

The 18–20 km discontinuity observable in each cross section (Fig. 5), beneath the Central and Western Precordillera, has been interpreted in previous studies as the main thrust between the thin-skinned deformed Precordillera and the Cuyania basement. Our stacked RFs allow us to better constrain the lateral extent of this structure both in the E–W and SE–NW directions. The relatively low S-wave velocity (∼3.4 km/s) mainly characterizing sedimentary rocks (Brocher, 2005) observed in Fig. 6 down to ∼20 km depth confirms a major lithology change at this depth.

Interestingly, we note that the regional seismicity (Linkimer, 2011; Marot et al., 2013; Venerdini et al., 2016) affects the crust mostly between ∼20 and ∼40 km corresponding to the two aforementioned discontinuities (Fig. 5 & 6c). Shear-wave velocities observed for these levels are comparable to those observed for the Sierra de Pie de Palo ($3.4 < V_s < 3.6$ km/s) which is consistent with a similar type of metamorphic rocks forming the Cuyania basement. The 40 km discontinuity coincides with a sharp decrease in seismic activity, which has been observed and interpreted as the brittle/ductile transition for the Cuyania terrane (Regnier et al., 1994; Ammirati et al., 2013).

All cross sections show major arrivals beneath the WSP (∼54 km), the Eastern Precordillera (53–55 km) and Central and Western Precordillera (∼65 km). In good agreement with previous studies, we interpret these arrivals as the Moho discontinuity. Fig. 5a exhibits quite an important jump in Moho depth (∼65 km beneath the Precordillera and ∼52 beneath the Eastern

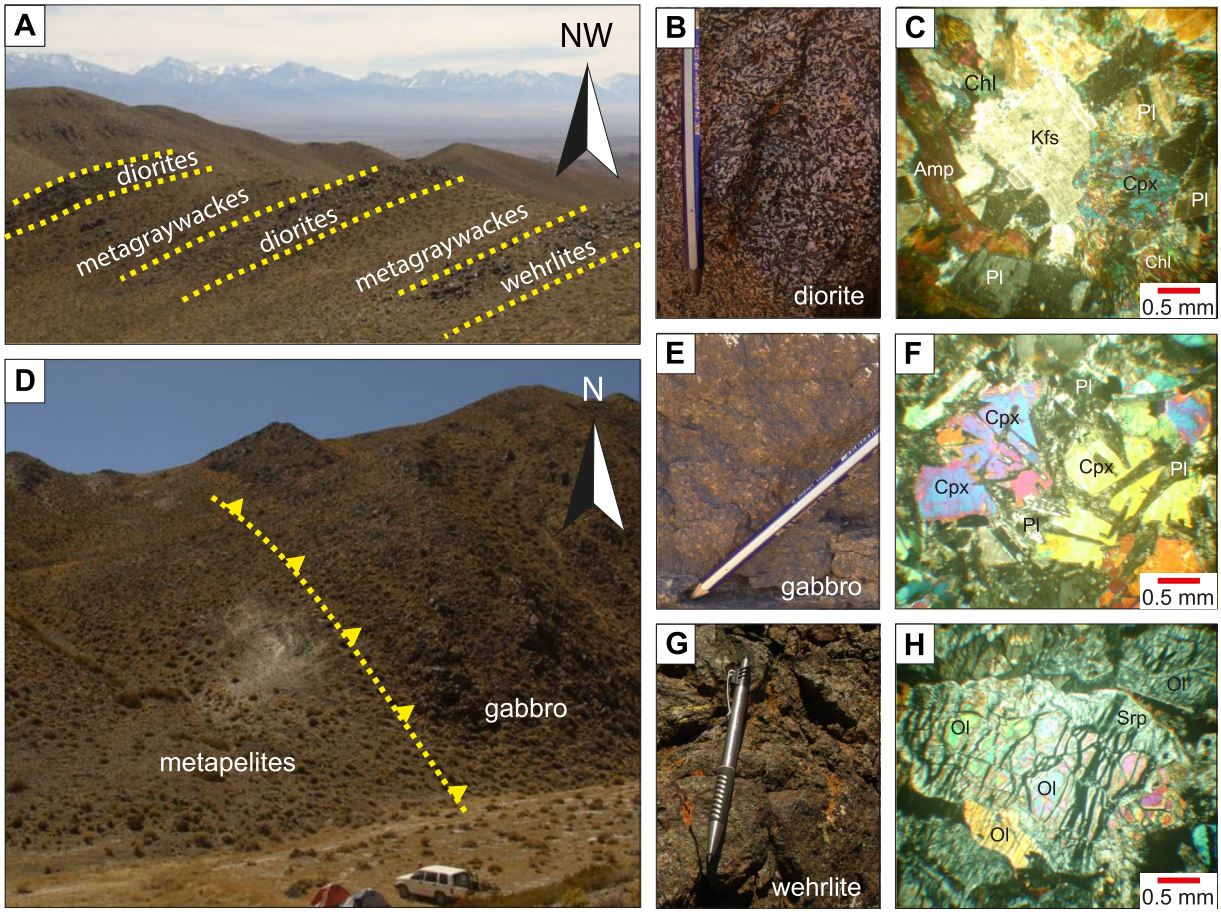

Fig. 7. A series of pictures from the Central Precordillera illustrating the mafic–ultramafic belt at the transition zone between the Chilenia and Cuyania terranes (Fig. 2). **A)** Thick diorite and wehrlite sills interlayered in metagraywacke layers. **B)** Diorite sample in hand. Primary minerals (mainly hornblende and plagioclase) can be easily recognized due to their coarse granular texture. **C)** Partially altered diorite sample under cross-polarized light showing the hipydiomorphic texture. Note the presence of primary (amphibole, plagioclase, clinopyroxene) and secondary minerals (such as chlorite) minerals. **D)** Gabbro sill in tectonic contact with metapelites layers. **E)** Massive gabbro with medium granular texture. **F)** Same sample as (E) in thin section under cross-polarized light. Note the presence of well-preserved primary minerals such as clinopyroxene and plagioclase showing ophitic and subophitic texture. **G)** Coarse granular wehrlite rock sample (Same as in A). **H)** Wehrlite sample in thin section under cross-polarized light showing alotriomorphic texture. Olivine is mostly altered to serpentine. Pl: plagioclase; Kfs: K-feldspar, Amp: amphibole, Ol: olivine; Cpx: clinopyroxene; Chl: chlorite; Srp: serpentine.

Precordillera). An interesting observation is the superposition of two Moho arrivals beneath the Central Precordillera (well visible in Fig. 5b). This double Moho configuration coincides with zones of particularly poor Moho signal observed in previous teleseismic RF studies (Gilbert et al., 2006; Ammirati et al., 2013) which had then been interpreted as partial eclogitization of the lower crust. Our high-resolution local RFs allow us to better resolve the Moho signal beneath the Central Precordillera, that would be in fact formed by two smaller arrivals at (60–65 km and 50–55 km). Although this double Moho could be a result of combining a complex 3D geometry and projection effects when realizing the cross section, Gans et al. (2011) and Ammirati et al. (2015) showed that in the flat slab region, the Moho is clearly and rather abruptly deepening to the west. Cross section C–D is quite perpendicular to the N–S structures that would affect the Moho geometry. Projection effects are thus unlikely.

We suggest that the double Moho signal could delimitate a zone where most of the Cuyania crustal material is turned to eclogites. Our absolute S-wave velocities of 4.2–4.3 km/s obtained for this zone are consistent with eclogites S-wave velocities (Christensen and Mooney, 1995). Previous observations from Gilbert et al. (2006), Porter et al. (2012) and Ammirati et al. (2015) at lithospheric scale also suggest that the flat slab is releasing water that could contribute to the lower crust eclogitization by migration from the slab to the base of the crust.

Our shear-wave velocities for depths greater than 40 km (>3.8 km/s) combined with petrological analyses (Pérez Luján et al., 2015) show that the Cuyania terrane mainly consists of mafic rocks (such as leuco-gabbros, gabbros, olivine-enriched gabbros and wherlites) (Fig. 7). The main mineral composition mostly consists in Ca-rich plagioclase (labradorite and bitownite) and clinopyroxene (diopside and augite). Primary mineral assemblage exhibits low pervasive alteration where plagioclase is variably altered to epidote, calcite, sericite and chlorite. Clinopyroxene is mostly fresh and sometimes presents rims of pseudomorphic tremolita and chlorite, which implies low-grade metamorphism.

Previous studies using microscopic Fourier transform infrared spectroscopy have revealed that clinopyroxene and plagioclase (nominally anhydrous minerals) commonly contain a significant amount of water as OH (Yang et al., 2008). The breakdown of plagioclase in gabbroic lithologies, favored by the presence of water, would drive to eclogitization (Hacker, 1996). In the Cuyania terrane, we expect partial eclogitization occurring deeper than 40 km with an increasing fraction of eclogite with increasing depth.

4.2. The Frontal Cordillera crust

Although some features of the Cordilleran crustal structure appear similar to the ones beneath the Precordillera, their interpreta-

tion diverges due to significant differences in terrane composition and geological history. Also, due to the restriction on the epicentral distance, stations in the Frontal Cordillera (GUAR, REGU and CASP) produce fewer RFs, which imply that the stacking may have not reduced the noise significantly. Although a poorer quality for the images obtained in this region, some features appear well identifiable and quite consistent with geological observations.

Cross sections in Fig. 5 at 69.4°W, show shallow arrivals at ∼5 km depth that could be related to the bottom of the thick Tertiary/Quaternary deposits filling the Uspallata–Calingasta valley. This 5-km depth conversion seems to extend and deepen to the west and merge with another arrival at 10 km depth (Fig. 5a & c). Both arrivals could be generated by the presence of the Frontal Cordillera thrust belt décollement (Heredia et al., 2002). Geological studies in the region indicate that the basement consists of a thick (∼2.5 km) rhyolitic sequence of lavas, ignimbrites and volcanoclastic sediments characterizing the Permian–Triassic Choiyoi Group, intruded by Triassic granitoids (Cristallini and Ramos, 2000; Giambiagi and Ramos, 2002; Rocher et al., 2015) (Fig. 2). We observe a major arrival at a depth of approximately 15 km (Fig. 5a & c) that seems to reach 20 km depth more in the south (Fig. 5b). Since there is no geological evidence for a drastic change in lithology at this depth and considering that the Chilenia basement is mainly composed of quartz enriched material (Cristallini and Ramos, 2000), we interpret this 15–20 km arrival as the brittle–ductile transition generally expected around such depths in quartz-enriched formations (granite and granodiorite).

In terms of absolute velocities (Fig. 6) we observe that lower shear-wave velocities at both shallow and deeper levels generally characterize the Frontal and Principal Cordillera crust. Between 0 and 10 km depths low shear-wave velocities (<3.4 km/s) characterize the intensely deformed Mesozoic sediments. We note that some shallow seismicity (Fig. 6c) in this area seems to coincide with the discontinuity at ∼10 km and would thus mark the main thrust décollement separating the deformed Mesozoic cover from the underlying basement. Relatively low S-wave velocities are observed in the Chilenia basement (∼3.5 km/s) down to 45–50 km depths, compatible with quartz-enriched material (Christensen and Mooney, 1995). A very clear arrival between 67 and 69 km on all studied cross sections (Fig. 5) corresponds to the Moho. These Moho depths are in good agreement with Gans et al. (2011) results although our higher resolution images allow for a sharper imaged Moho conversion.

At depth, the increase in crustal pressure and temperature (200 MPa – 550 °C at the base of the crust, according to Marot et al., 2014) will eventually allow the transition to felsic granulite and/or eclogites. We believe that this transition occurs at 50–55 km since all cross sections show arrivals at this depth. We also observe a significant increase in shear-wave velocities (from 3.6 to >3.8 km/s) compatible with an eclogite facies beneath the Principal and Frontal Cordillera.

Interestingly, comparing our results with recorded seismicity shows a cluster of seismic activity around 70.2°W (Fig. 6c). We believe that this seismicity is related to the presence of the La Ramada thrust belt affecting the Principal Cordillera with a discontinuity at ∼10 km separating the Mesozoic strata from the basement and a décollement level at ∼20 km depth that coincides with the brittle–ductile transition, in good agreement with Cristallini and Ramos (2000).

4.3. The Cuyania–Chilenia terrane boundary

In the south central Andes, the evolutional history for the western margin of Gondwana is still widely debated and mostly depends on the presence (or absence) of a Devonian magmatic arc

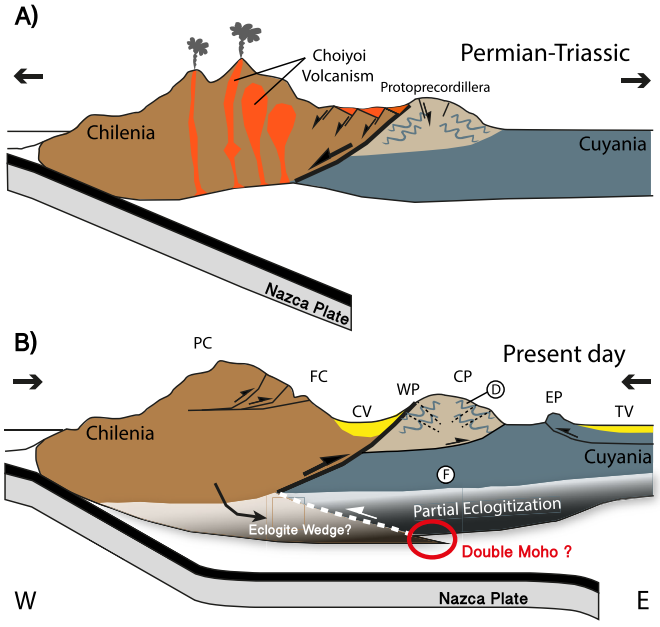

Fig. 8. A) Western margin of Gondwana during the Permian–Triassic in the region of study. Choiyoi volcanism probably changed the composition of the Chilenia terrane and contributed to its expansion. Extensional stresses due to the break-up of Gondwana led to normal faulting. The master structure suggested by the geophysical analyses in this work is a good candidate to accommodate the extension between Cuyania and Chilenia also controlling the deposition of the Choiyoi Group on the Chilenia side. **B)** Present day western margin of South America at ∼31–32°S. As a result of 20 Ma of Andean compression, previous structures may have been reactivated as reverse faults. Simultaneously, the region recorded slab flattening coeval with the uplift of the Eastern Precordillera and Sierras Pampeanas (more to the east). PC: Principal Cordillera, FC: Frontal Cordillera, CV: Calingasta valley, WP: Western Precordillera, CP: Central Precordillera, EP: Eastern Precordillera, TV: Tulum valley. Circled letters refer to the lithology described in Fig. 7.

between the Chilenia and Cuyania terranes. At 31–32°S, there is no evidence for such magmatism. Moreover, Ordovician basalts in the Calingasta and Rodeo areas (Fig. 2) present geochemical characteristics of early stages of extending oceanic ridge magmatism (Kay et al., 1984), which suggests that the Chilenia and Cuyania terranes were probably part of the same block that spread apart during the Ordovician. The extension probably resulted in subsidence and areas of low elevation that were filled with the fine sedimentary material interlayered with the mafic–ultramafic outcrops observable in the current Western and Central Precordillera (Fig. 7). Extension in this region, however, was probably not significant enough to generate oceanic crust. During the Late Ordovician, when the eastern margin of the Chilenia–Cuyania block docked to the western margin of Gondwana, the extension stopped and the ocean recently formed between the Chilenia and Cuyania terranes would have closed without generating arc-type magmatism. The low metamorphic grade and the double vergence observed by Pérez Luján et al. (2015) in the Sierra de la Invernada and Rodeo area (Fig. 2) supports this hypothesis of a narrow ocean closed by the tectonic inversion of previous extensional structures at this latitude. We believe that our RF results presented in the previous section allowed us to identify one of these structures (Fig. 5 & 6). This would be a major Ordovician west-dipping master fault affecting the whole crust and then inverted in reverse faulting from late Ordovician to Middle Devonian, driving to the formation of a proto-Precordillera (current Western and Central Precordillera). Under compression, this structure would lead the Cuyania basement under the Chilenia basement in a continental collision.

Later, the Chilenia terrane recorded intense orogenic magmatism as suggested by the presence of the Permian–Triassic Choiyoi

Group (Fig. 8a). The Choiyoi is almost absent in the Precordillera, east of the Uspallata–Calingasta valley. The presence of a major west-dipping structure between the Frontal Cordillera and the Precordillera is consistent with this observation. The Choiyoi Group has been defined as a volcanic complex developed in extensional conditions whose emplacement and deposition occurred in a series of half-grabens controlled by normal faults with downthrown western blocks (Heredia et al., 2002). In the Frontal Cordillera, the Choiyoi Group is more than 2.5 km thick and associated with large granitic plutons (Heredia et al., 2002; Rocher et al., 2015). In contrast, the Precordillera, Permian–Triassic magmatic rocks are very scarce and mostly restricted to the southern Precordillera of Mendoza at ∼33°S (Strazzere et al., 2006). The structure recognized in this work could have played an important role during the Permian–Triassic, accommodating extensional tectonics between Cuyania and Chilenia (Fig. 8a). In this scenario the magmatic activity and extensional deformation mainly affected the hanging-wall, which in this case corresponds to the Frontal Cordillera (Chilenia), leaving the foot–wall (Cuyania) less affected by the Choiyoi magmatism (e.g. Ebinger and Casey, 2001). Also, the Choiyoi magmatism probably changed the composition of the Chilenia basement by intrusion of quartz-enriched material (Rocher et al., 2015) and more importantly, probably contributed to the creation of new, granitic continental crust.

During the Miocene, the Andean compression inverted previous structures both inherited from the Ordovician and the Permian–Triassic. The important shallow seismic activity recorded in the region (Fig. 6c) demonstrates that this global shortening is still active. We suggest that our Ordovician master structure has been reactivated in reverse faulting and accommodates crustal deformation down to ∼40 km depth by thrusting the Chilenia terrane over the Cuyania terrane. Reverse focal mechanisms for crustal intermediate magnitude earthquakes (Alvarado et al., 2010; Ammirati et al., 2015) support this hypothesis. Moreover we observe a cluster of seismicity around (69.3°W) presenting a west-dipping trend at the transition zone between the Cuyania and Chilenia terranes where our master structure is expected.

Although not very well constrained, some features suggested by our seismic results allow us to propose a hypothesis that supports shortening mechanisms in the lower crust. The possibility exists that the described west-dipping Ordovician structure would affect the whole crust by simple shear thrusting. However in this case, Moho deformation should be observed beneath the Frontal and Principal Cordillera as observed in other orogens (e.g. Giese et al., 1999; Zangh et al., 2014). Also, because our structure would drive Cuyanian material to the west, under the Chilenia terrane, it would be difficult to explain the abnormally thick crust observed beneath the Central Precordillera. According to Allmendinger and Judge (2014), this phenomenon could rather be explained by an eastward material transference possibly driven by subduction erosion. The presence of a double Moho beneath the Precordillera (Fig. 5) would provide more constraints about such a process. To accommodate material transference from Chilenia under the Cuyania terrane, we need an east-dipping shearing structure that would connect the bottom of our aforementioned Ordovician master fault to the double Moho inferred from our local RF analysis (Fig. 5 & 6). Our hypothesis thus involves an eclogite wedge migrating eastward from the Chilenia lower crust underneath the Cuyania terrane accommodating shortening in the lower crust. Under compression, as the Cuyania terrane remains rigid down to ∼40 km depth, it would act like a “planer”, cutting through the much softer Chilenia terrane. Below 40 km, both Cuyania and Chilenia lower crust are likely turned into eclogites that would be driven to the east by subduction erosion contributing to the crustal thickening observed beneath the Central Precordillera (Fig. 8b).

5. Conclusions

In this study, we computed high-resolution local receiver functions from slab seismicity in the Pampean flat slab region of Argentina. The RFs have been stacked to produce 2D cross sections imaging the velocity structure and their lateral extent across the region of study. Then, we jointly inverted phase velocity dispersion with our local RFs to constrain high-resolution absolute shear-wave velocity structure and combined them with our stacked RFs images. Our improved level of crustal details allowed us to better constrain regional tectonic features such as décollement levels accommodating regional crustal shortening as well as small structures related to very shallow changes in lithology such as sedimentary basins (Tulum Valley, Calingasta Valley).

We suggest the presence of a major structure that separates the Cuyania and Chilenia terranes. We geometrically constrained this structure using the crustal seismicity recorded by several seismic experiments deployed in the region and focal mechanisms from regional moment tensor inversion. This structure is well constrained down to ∼40 km depth, dipping to the west and exhibiting reverse motion. Petrological analyses show that the Precordillera recorded evidence of extension during the Late Ordovician with spreading ridge magmatism. From Late Ordovician to Middle Devonian, this narrow ocean was closed, probably by the tectonic inversion of one major extensional structure leading to the collision of the Chilenia and Cuyania terranes. This structure would correspond to the one observed in our stacked RFs images. The collision between the two terranes likely led to crustal thickening. The Permian–Triassic extension in the region considerably changed the geological configuration. At this time, Chilenia recorded intense magmatism that contributed to its expansion and a major change of its rock composition probably due to the creation of new granitic crust. This major structure apparently played an important role in controlling the regional deformation during the Permian–Triassic. To explain crustal shortening accommodation in the lower crust, we propose the hypothesis of an eclogite wedge migrating from Chilenia beneath Cuyania contributing to the complex Moho geometry and the abnormally high crustal thickness generally observed beneath the Precordillera and western Sierras Pampeanas.

Acknowledgements

This work has been supported by the Ministerio de Ciencia, Tecnología e Innovación Productiva of Argentina (PICT2011-160). We thank Ryan Porter for providing with the ANT dispersion data used in this work. We are grateful to the Incorporated Research Institutions for Seismology (IRIS) for the easy download of the data presented in this study. The SIEMBRA project was supported by the National Science Foundation of the USA (NSF, EAR 0510966 and 0907880). We also thank Suzanne M. Kay, Brian Horton and Chelsea Mackaman-Lofland for constructive discussions about the geochemistry of the Western Precordillera and suggestions of very useful references. Most of the figures presented in this manuscript were made using the Generic Mapping Tools (GMT). The joint inversion of RF and Surface wave dispersion has been performed using the Computer Programs in Seismology (CPS) package, version 3.30 and the Seismic Analysis Code (SAC). We particularly thank the editor, Peter Shearer as well as two anonymous reviewers for their very helpful comments.

Appendix A. Supplementary material

Supplementary material related to this article can be found online at http://dx.doi.org/10.1016/j.epsl.2016.06.018.

References

Allmendinger, R.W., Figueroa, D., Snyder, D., Beer, J., Mpodozis, C., Isacks, B.L., 1990. Foreland shortening and crustal balancing in the Andes at 30°S latitude. Tectonics 9, 789–809.

Allmendinger, R.W., Judge, P.A., 2014. The Argentine Precordillera: a foreland thrust belt proximal to the subducted plate. Geosphere 10 (6), 1203–1218. http://dx.doi.org/10.1130/GES01062.1.

Alvarado, P., Sánchez, G., Saez, M., Castro de Machuca, B., 2010. Nuevas evidencias de la actividad sísmica del terreno Cuyania en la región de subducción de placa horizontal de Argentina. Rev. Mex. Cienc. Geol. 27 (2), 278–291.

Ammirati, J.-B., Alvarado, P., Perarnau, M., Saez, M., Monsalvo, G., 2013. Crustal structure of the Central Precordillera of San Juan, Argentina (31°S) using teleseismic receiver functions. J. South Am. Earth Sci. 46, 100–109. http://dx.doi.org/10.1016/j.jsames.2013.05.007.

Ammirati, J.-B., Alvarado, P., Beck, S., 2015. A lithospheric velocity model for the flat slab region of Argentina from joint inversion of Rayleigh wave phase velocity dispersion and teleseismic receiver functions. Geophys. J. Int. 202, 224–241. http://dx.doi.org/10.1093/gji/ggv140.

Anderson, M., Alvarado, P., Zandt, P., Beck, S., 2007. Geometry and brittle deformation of the subducting Nazca Plate, Central Chile and Argentina. Geophys. J. Int. 171, 419–434. http://dx.doi.org/10.1111/j.1365-246X.2007.03483.x.

Baldis, B., Beresi, M., Bordonaro, O., Vaca, A., 1982. Síntesis evolutiva de la Precordillera Argentina. In: 5° Congres Latinoam. Geol., Actas 4. Buenos Aires, Argentina, pp. 399–445.

Boedo, F.L., Vujovich, G.I., Kay, S.M., Ariza, J.P., Pérez Luján, S.B., 2013. The E-MORB like geochemical features of the Early Paleozoic mafic–ultramafic belt of the Cuyania terrane, Western Argentina. J. South Am. Earth Sci. 48, 73–84.

Brocher, T.M., 2005. Empirical relations between elastic wavespeeds and density in the Earth's crust. Bull. Seismol. Soc. Am. 95, 2081–2092. http://dx.doi.org/10.1785/0120050077.

Cahill, T., Isacks, B.L., 1992. Seismicity and the shape of the subducted Nazca plate. J. Geophys. Res. 97, 17503–17529. http://dx.doi.org/10.1029/92JB00493.

Calkins, J., Zandt, G., Gilbert, H., Beck, S., 2006. Crustal images from San Juan, Argentina, obtained using high frequency local event receiver functions. Geophys. Res. Lett. 33, 1–4. http://dx.doi.org/10.1029/2005GL025516.

Castro de Machuca, B., Perarnau, M., Alvarado, P., López, G., Saez, M., 2012. A seismological and petrological crustal model for the southwest of the Sierra de Pie de Palo, Province of San Juan. Rev. Asoc. Geol. Argent. 69, 179–186.

Christensen, N.I., Mooney, W.D., 1995. Seismic velocity structure and composition of the continental crust: a global view. J. Geophys. Res. 100, 9761–9788. http://dx.doi.org/10.1029/95JB00259.

Cristallini, E.O., Ramos, V.A., 2000. Thick-skinned and thin-skinned thrusting in the La Ramada fold and thrust belt: crustal evolution of the high Andes of San Juan, Argentina (32°SL). Tectonophysics 317, 205–235. http://dx.doi.org/10.1016/S0040-1951(99)00276-0.

Davis, J.S., Roeske, S.M., McClelland, W.C., Snee, L.W., 1999. Closing the ocean between the Precordillera terrane and Chilenia: early Devonian ophiolite emplacement and deformation in the southwest Precordillera. In: Ramos, V.A., Keppie, J.D. (Eds.), Laurentia Gondwana Connections Before Pangea. In: Geol. Soc. Am. Special Paper, vol. 336. Geol. Soc. Am., Boulder, Colorado, USA, pp. 115–138.

Dueker, K.G., Sheehan, A.F., 1997. Mantle discontinuity structure from midpoint stacks of converted P to S waves across the Yellowstone hotspot track. J. Geophys. Res. 102, 8313–8327.

Ebinger, C.J., Casey, M., 2001. Continental breakup in magmatic provinces: an Ethiopian example. Geology 29 (6), 527–530. http://dx.doi.org/10.1130/0091-7613(2001)029<0527:CBIMPA>2.0.CO;2.

Gans, C.R., Beck, S.L., Zandt, G., Gilbert, H., Alvarado, P., Anderson, M., Linkimer, L., 2011. Continental and oceanic crustal structure of the Pampean flat slab region, western Argentina, using receiver function analysis: new high-resolution results. Geophys. J. Int. 186, 45–58. http://dx.doi.org/10.1111/j.1365-246X.2011.05023.x.

Giambiagi, L.B., Ramos, V.A., 2002. Structural evolution of the Andes in a transitional zone between flat and normal subduction (33°30′–33°45′S), Argentina and Chile. J. South Am. Earth Sci. 15, 101–116.

Giese, P., Scheuber, E., Schilling, F., Schmidz, M., Wigger, P., 1999. Crustal thickening processes in the Central Andes and the different natures of the Moho-discontinuity. J. South Am. Earth Sci. 12, 201–220. http://dx.doi.org/10.1016/S0895-9811(99)00014-0.

Gilbert, H., Beck, S., Zandt, G., 2006. Lithospheric and upper mantle structure of central Chile and Argentina. Geophys. J. Int. 165, 383–398. http://dx.doi.org/10.1111/j.1365-246X.2006.02867.x.

Gurrola, H., Minster, J.B., Owens, T., 1994. The use of velocity spectrum for stacking receiver functions and imaging upper mantle discontinuities. Geophys. J. Int. 117, 427–440.

Hacker, B.R., 1996. Eclogite formation and the rheology, buoyancy, seismicity, and H_2O content of oceanic crust. In: Geophysical Monograph, vol. 96. American Geophysical Union, Washington D.C., USA, pp. 337–346.

Heredia, N., Rodríguez Fernández, L.R., Gallastegui, G., Busquets, P., Colombo, F., 2002. Geological setting of the Argentine Frontal Cordillera in the flat-slab segment (30°00′–31°30′S latitude). J. South Am. Earth Sci. 15, 79–99.

Herrmann, R.B., Ammon, C.J., 2002. Computer programs in seismology – 3.30: surface waves, receiver functions and crustal structure. www.eas.slu.edu/People/RBHerrmann/CPS330.html.

Julià, J., Ammon, C.J., Herrmann, R.B., Correig, A.M., 2000. Joint inversion of receiver function and surface wave dispersion observations. Geophys. J. Int. 143, 99–112.

Kay, S.M., Ramos, V.A., Kay, R.W., 1984. Elementos mayoritarios y trazas de las vulcanitas ordovícicas de la Precordillera Occidental: Basaltos de rift oceánico temprano (?) próximos al margen continental. In: IX Congreso Geológico Argentino, Actas II. S.C. de Bariloche, Rio Negro, Argentina, pp. 48–65.

Kay, S., Abbruzzi, J., 1996. Magmatic evidence for Neogene lithospheric evolution of the Central Andean flat-slab between 30 and 32°S. Tectonophysics 259, 15–28. http://dx.doi.org/10.1016/0040-1951(96)00032-7.

Kay, S.M., Orrell, S., Abbruzzi, J.M., 1996. Zircon and whole rock Ns–Pb isotopic evidence for a Greenville age and Laurentia origin for the basement of the Precordilleran Terrane in Argentina. Geol. Soc. Am. South-Central Sec. Abs. Prog. 28 (1), 21–22.

Langston, C.A., 1979. Structure under Mount Rainier, Washington, inferred from teleseismic body waves. J. Geophys. Res. 84, 4749–4762.

Ligorría, J., Ammon, C.J., 1999. Iterative deconvolution and receiver function estimation. Bull. Seismol. Soc. Am. 89, 1395–1400.

Linkimer, L., 2011. Lithospheric structure of the Pampean flat slab (latitude 30–33°S) and Northern Costa Rica (latitude 9–11°N) subduction zones. Dissertation (PhD). University of Arizona, Tucson, Arizona, USA.

Marot, M., Monfret, T., Pardo, M., Ranalli, G., Nolet, G., 2013. A double seismic zone in the subducting Juan Fernández Ridge of the Nazca Plate (32°S), central Chile. J. Geophys. Res. 118 (7), 3462–3475. http://dx.doi.org/10.1002/jgrb.50240.

Marot, M., Monfret, T., Gerbault, M., Nolet, G., Ranalli, G., Pardo, M., 2014. Flat versus normal subduction zones: a comparison based on 3-D regional traveltime tomography and petrological modelling of central Chile and western Argentina (29°–35°S). Geophys. J. Int. 199, 1633–1654. http://dx.doi.org/10.1093/gji/ggu355.

Mulcahy, P., Chen, C., Kay, S.M., Brown, L.D., Isacks, B.L., Sandvol, E., Heit, B., Yuan, X., Coira, B.L., 2014. Central Andean mantle and crustal seismicity beneath the Southern Puna plateau and the northern margin of the Chilean–Pampean flat slab. Tectonics 33 (8), 1636–1658. http://dx.doi.org/10.1002/2013TC003393.

Perarnau, M., Alvarado, P., Saez, M., 2010. Estimación de la estructura cortical de velocidades sísmicas en el suroeste de la Sierra de Pie de Palo, Provincia de San Juan. Rev. Asoc. Geol. Argent. 64, 473–480.

Perarnau, M., Gilbert, H., Alvarado, P., Martino, R., Anderson, M., 2012. Crustal structure of the Eastern Sierras Pampeanas of Argentina using high frequency local receiver functions. Tectonophysics 580, 208–217. http://dx.doi.org/10.1016/j.tecto.2012.09.021.

Pérez Luján, S.B., Ammirati, J.-B., Alvarado, P., Vujovich, G.I., 2015. Constraining a mafic thick crust model in the Andean Precordillera of the Pampean flat slab subduction region. J. South Am. Earth Sci. 64, 325–338. http://dx.doi.org/10.1016/j.jsames.2015.09.005.

Porter, R., Gilbert, H., Zandt, G., Beck, S., Warren, L., Calkins, J., Alvarado, P., Anderson, M., 2012. Shear wave velocities in the Pampean flat-slab region from Rayleigh wave tomography: implications for slab and upper mantle dehydration. J. Geophys. Res. 117. http://dx.doi.org/10.1029/2012JB009350.

Ragona, D., Anselmi, G., Gonzaléz, P., Vujovich, G., 1995. Mapa geológico de la provincia de San Juan. República Argentina, Secretaría de Minería, Dirección Nacional del Servicio Geológico, Buenos Aires, Argentina.

Ramos, V.A., 1988. The tectonics of the Central Andes: 30° to 33°S latitude. In: Clark, S.P., Clark Burchfiel, J.B., Suppe, J. (Eds.), Processes in Continental Lithospheric Deformation. Geological Society of America, pp. 31–54.

Ramos, V.A., Cristallini, E.O., Pérez, D.J., 2002. The Pampean flat-slab of the central Andes. J. South Am. Earth Sci. 15, 59–78.

Regnier, M., Chiu, J.-M., Smalley, R., Isacks, B.L., Araujo, M., 1994. Crustal thickness variation in the Andean foreland, Argentina, from converted waves. Bull. Seismol. Soc. Am. 84 (4), 1097–1111.

Rocher, S., Vallecillo, G.M., Castro de Machuca, B., Alasino, P.H., 2015. El Grupo Choiyoi (Pérmico temprano-medio) en la Cordillera Frontal de Calingasta, San Juan, Argentina: Volcanismo de arco asociado a extensión. Rev. Mex. Cienc. Geol. 32 (3), 415–432.

Stauder, W., 1973. Mechanism and spatial distribution of Chilean earthquakes with relation to subduction of the oceanic plate. J. Geophys. Res. 78, 5033–5061. http://dx.doi.org/10.1029/JB078i023p05033.

Strazzere, L., Gregori, D.A., Dristas, J.A., 2006. Genetic evolution of Permo–Triassic volcaniclastic sequences at Uspallata, Mendoza Precordillera, Argentina. Gondwana Res. 9, 485–499. http://dx.doi.org/10.1016/j.gr.2005.12.003.

Venerdini, A., Sánchez, G., Alvarado, P., Bilbao, I., Ammirati, J.-B., 2016. Nuevas determinaciones de velocidades de ondas P y ondas S para la corteza sísmica del terreno Cuyania en el retroarco andino. Rev. Mex. Cienc. Geol. 33 (1), 59–71.

Wagner, L.S., Beck, S., Zandt, G., 2005. Upper mantle structure in the south central Chilean subduction zone (30° to 36°S). J. Geophys. Res. 110. http://dx.doi.org/10.1029/2004JB003238.

Yáñez, G., Cembrano, J., Pardo, M., Ranero, C., Selles, D., 2002. The Challenger-Juan Fernández – Maipo major tectonic transition of the Nazca–Andean subduction system at 33–34°S: geodynamic evidence and implications. J. South Am. Earth Sci. 15, 23–38.

Yang, X., Deloule, E., Xia, Q., Fan, Q., Feng, M., 2008. Water contrast between Pre-

cambrian and Phanerozoic continental lower crust in eastern China. J. Geophys. Res. 113, B08207.

Zangh, Z., Wang, Y., Houseman, G.A., Xu, T., Wu, Z., Yuan, X., Chen, Y., Tian, X., Bai, Z., Teng, J., 2014. The Moho beneath western Tibet: Shear zones and eclogitization in the lower crust. Earth Planet. Sci. Lett. 408, 370–377. http://dx.doi.org/10.1016/j.epsl.2014.10.022.